Computational and Theoretical Chemistry 1225 (2023) 114135

Contents lists available at ScienceDirect

Computational and Theoretical Chemistry

journal homepage: www.elsevier.com/locate/comptc

# Theoretical insights on pyrene end-capped thiophenes/furans and their suitability towards optoelectronic applications

Arka Bhattacharya, Periyasamy Angamuthu Praveen, Sreegowri V. Bhat, Saravanapriya Dhanapal, Arulkannan Kandhasamy, Thangavel Kanagasekaran *

*Organics Optoelectronics Laboratory, Department of Physics, Indian Institute of Science Education and Research - Tirupati, Tirupati, India*

ARTICLE INFO

*Keywords:*
Organic semiconductors
Organic photovoltaics
Solar cells
OLETs
DFT
Charge transfer
TDDFT
Excited state

ABSTRACT

Organic semiconductors are attractive candidates for the development of flexible and efficient optoelectronic devices. In this work, we have studied the pyrene end-capped thiophene derivatives with different number of oligomeric rings and substituted with their oxygen analogue furan. Results indicate that the molecular planarity varies with the substitution of furan rings and the number of rings play a role on optoelectronic property of the systems. All the systems have shown ambipolar behavior, but the high charge barrier in the case of electrons could limit the device performance. Further, in photovoltaic analysis the increment in oligomeric ring has substantially reduces the open circuit voltage and the fill factor. However, the introduction of furan has improved the overall light harvesting efficiency. With the proper choice of material and device engineering the shorter systems can be considered for photovoltaics, where as the longer derivatives can be considered for light emitting device applications.

## 1. Introduction

Organic semiconductors are one of the rapidly growing field of interests owing to their structural tunability, ease in processability and low synthetic costs. Since, literally it is possible to fabricate these materials on any substrate, there is great surge of interest to develop flexible organic electronic devices. Already, organic light emitting diodes are proven as a better candidates for flexible display technology and offers high contrast, crisp and vivid pixels than their inorganic counterparts. Presently, there is an intensive exploration in the sister fields such as organic field effect transistors (OFET), organic photodetectors, memory devices and organic photovoltaic (OPV) cells [1–5]. These fields are in requirement of new promising materials with high mobility and tunable exciton dynamics. Especially, since these materials can be fabricated as ambipolar semiconductors, there opens a possibility to develop organic light emitting transistors (OLET) and then to the long sought organic lasers [5–8]. On the other hand, by properly controlling the exciton dynamics, these materials can be utilized for the development of OPV devices [9–11].

In this regard, linearly fused aromatic compounds such as tetracene, pentacene, rubrene and oligothiophenes are widely investigated in the form of OFETs and OPVs [12–15]. Particularly, oligothiophenes are one of the promising and widely studied moieties in terms of organic electronic materials. The thiophenes, when combined with different oligomer lengths, proper side chains and terminal groups can be tuned to achieve a specific property such as specific absorption or emission wavelength. Due to this advantage thiophene derivatives are synthesized and studied for electronic and optoelectronic applications [16–19]. Particularly, when the thiophenes are end-capped with pyrene results planar conjugated, electron rich molecules with strong $\pi$-delocalization and high fluorescence emission [20,21]. Few reports already demonstrated the feasibility of these systems towards the fabrication of OLETs with moderate mobility and photoluminescence quantum yield (PLQY) [22,23]. The presence of sulfur atom in the thiophene core gives rise of strong intermolecular interactions leads to high mobility. On the other hand, the large size and small electronegativity of sulfur affects the molecular planarity and crystal packing. Further, often a heavy atom effect due to the presence of sulfur has been observed in thiophene based systems. One way to overcome such difficulties is by the substitution of thiophene moieties by furan [24]. Furan is an oxygen analogue of thiophene with larger electronegativity and smaller covalent radius than sulfur and due to this, it offers the shortening of $\pi - \pi$ stacking distance leads to an improved charge carrier transport and optical properties [25]. Further, replacing sulfur with oxygen would help to tune the highest occupied molecular orbital (HOMO), lowest unoccupied molecular orbital (LUMO) and energy gaps of the accompanying molecular system. Since, the furan moieties

* Corresponding author.
*E-mail addresses:* praveen@iisertirupati.ac.in (P.A. Praveen), kanagasekaran@iiseritupati.ac.in (T. Kanagasekaran).

https://doi.org/10.1016/j.comptc.2023.114135
Received 9 March 2023; Received in revised form 19 April 2023; Accepted 23 April 2023
Available online 27 April 2023

offers strong fluorescence emission, they are particularly of very interest towards OLET applications [19]. The smaller size of oxygen than sulfur is advantageous to reduce steric hindrance and thus improve the molecular planarity and crystal packing suitable for OPV. Additionally furan-based systems are comparatively more soluble than the thiophene based systems. So, using these system, devices can be fabricated by means of chemical or solution processing techniques, rather than the usual thermal assisted process. Finally, furan is abundant and can be naturally obtained from furfural polymer collected from trees and vegetables. So, these systems could be used towards the development of eco-friendly electronic devices [26].

In the present work, we have analyzed the bipyrene end-capped thiophene of different oligomer lengths (n = 1–3). These systems are already studied towards OFET and OLET applications and reported to have moderate mobility and PLQY [22]. We have substituted the furan moieties in the place of thiophene and studied their structural, electronic and optical properties. Further, a systematic analysis was carried out to evaluate their suitability towards OLET and OPV applications. We have observed that the furan substitution greatly improves the molecular planarity and hole mobility. Overall, the bipyrene end-capped systems show moderate OLET properties along with good OPV parameters indicating their suitability towards optoelectronic applications.

## 2. Methodology

In the present study we have considered three pyrene end-capped thiophenes, such as 2,5-bis(pyren-1-yl)thiophene (BPY1T), 5-(pyren-1-yl)-5′-(pyren-2-yl)-2,2′-bithiophene (BPY2T) and 5-(pyren-1-yl)-5′-[5-(pyren-1-yl)thiophen-2-yl]-2,2′-bithiophene (BPY3T) for the analysis. The molecular structures are retrieved from the previous report [22]. In each system the thiophene unit was replaced by the furan and the corresponding molecules are 2,5-bis(pyren-1-yl)furan (BPY1F), 5-(pyren-1-yl)-5′-(pyren-2-yl)-2,2′-bifuran (BPY2F) and 5-(pyren-1-yl)-5′-[5-(pyren-1-yl)furan-2-yl]-2,2′-bifuran (BPY3F). All the calculations were performed at B3LYP level with the 6-31G(d,p) basis set. The choice of the basis set is based on the fact that the availability of other similar reports for benchmarking and comparison [27–30]. For electronic calculations Gaussian 09 suite was used and for excited state analysis ORCA package has been utilized. In the case of ORCA, Gaussian equivalent basis set was used for the geometry optimization and the structure is compared with the Gaussian results [18,19]. Ideally, these results would be same and in such case excited state analysis are carried out.

In this work, the charge transport characteristics are modeled as the hopping process between two molecules. The charge carrier transport can be interpreted as charge mobilities and these values indicate how fast an charge carrier (hole or electron) move from one molecule to another molecule. Higher the hole mobility, the system is termed as p-type and higher the electron mobility, termed as n-type. In such a case, the hopping between two identical molecules can be expressed as $M^{\pm} \cdots \rightarrow M \ldots M^{\pm}$. Due to the charge injection, the molecule will undergo a structural relaxation to obtain an optimum structure in the charged state. This distorted molecules are termed as a polaron. By transferring the charge to the neighboring molecule, the first molecule tends to retain it original geometry and the neutral state.

In order to model the electron and hole mobility two molecular parameters, (a) reorganization energy and (b) charge transfer integral, are required. These two parameters are used to describe the charge transfer rate k as [31],

$$k = \frac{4\pi^2}{h} \frac{J_e^{\pm 2}}{\sqrt{4\pi\lambda^{\pm} k_B T}} \exp\left(-\frac{\lambda^{\pm}}{4k_B T}\right) \quad (1)$$

here $\lambda^{\pm}$ is the reorganization energy for hole or electron, $J_e^{\pm}$ is the transfer integral for hole or electron, h is Planck's constant, T is the temperature (298 K in our case) and $k_B$ is the Boltzmann constant. The reorganization energy can be calculated from the difference between neutral and charged state of a single molecule. The transfer integrals are obtained by modeling the dimers of the molecule. According to Marcus theory, reorganization energy is the measure of energy variation in a molecule due to its structural change when add or removing a charge carrier. Usually it is expressed as inner sphere and outer sphere reorganization energy values. But, it requires large computational cost to calculate the outer sphere reorganization energies as the electronic polarization and electron–phonon coupling of the surrounding molecules need to be considered. Due to its negligible values, in the present case we have considered only the inner reorganization energy values for the mobility calculations. It can be given as [32],

$$\lambda^{\pm} = \lambda_1^{\pm} + \lambda_2^{\pm} \quad (2)$$

here ± corresponds to the electron (–) or hole (+) state values and the $\lambda_1^{\pm}$ and $\lambda_2^{\pm}$ values can be directly calculated from the difference in adiabatic potential energy surfaces as,

$$\lambda_1^{\pm} = E_2^{\pm} - E_3^{\pm} \quad (3)$$

$$\lambda_2^{\pm} = E_4^{\pm} - E_1^{\pm} \quad (4)$$

where, $E_1^{\pm}$ is the neutral state energy of the optimized geometry, $E_2^{\pm}$ is the energy of the charged state in optimized geometry, $E_3^{\pm}$ is the energy of the charged optimized geometry and $E_4^{\pm}$ is the energy of the neutral state in charged geometry.

The charge transfer integral is a measure on strength of interaction between the dimers. In the present work, we are assuming the co-facial geometry for the analysis [31]. When two localized monomers are used to create the dimer, the highest occupied molecular orbital (HOMO) or the lowest unoccupied molecular orbital (LUMO) are combined together to form the HOMO and HOMO-1 (or LUMO and LUMO+1) state in dimer configuration. By using the energy splitting in dimer method, the charge transfer integral can be approximated as,

$$J_e^{\pm} = \left(\frac{E_{HOMO} - E_{HOMO-1}}{2}\right) \quad (5)$$

This method is accurate as long as the monomers are identical and are symmetrically positioned. By substituting the values of $\lambda$ and $J_e$ in Eq. (2), the charge transfer rate can be estimated. Further, by substituting the k values into Einstein's relation, the charge transfer mobility can be calculated as,

$$\mu = \frac{ed^2k}{2k_B T} \quad (6)$$

where d is the distance between two identical molecules in dimer state and e is the electronic charge. As noted, depending on the $\lambda$ and $J_e$ values, overall mobility of the system will be varied. Ideally, higher $J_e$ and lower $\lambda$ values are required to get efficient charge transport and high mobility in the system.

For the analysis of emission properties, the excited state analysis was carried out using the ORCA program and the results are then fed into an in-built advanced spectral analysis (ASA) module. Detailed description about this approach can be found elsewhere [33]. In simple terms, the vibrational structure of the electronic transitions are neglected and each individual electronic band is approximated as a Gaussian or Lorentzian or mixed lineshape. So, the electronic transition spectrum will depend on the applied field (or energy of the incident photon), electronic transition energy and the transition dipole moment. By choosing the optimal linewidth and the standard deviation parameters, corresponding absorption and emission spectrum are calculated.

## 3. Results and discussion

### 3.1. Structural analysis

The optimized geometries of the pyrene end-capped thiophenes and furans are given in Fig. 1. It can be seen from the geometries that upon

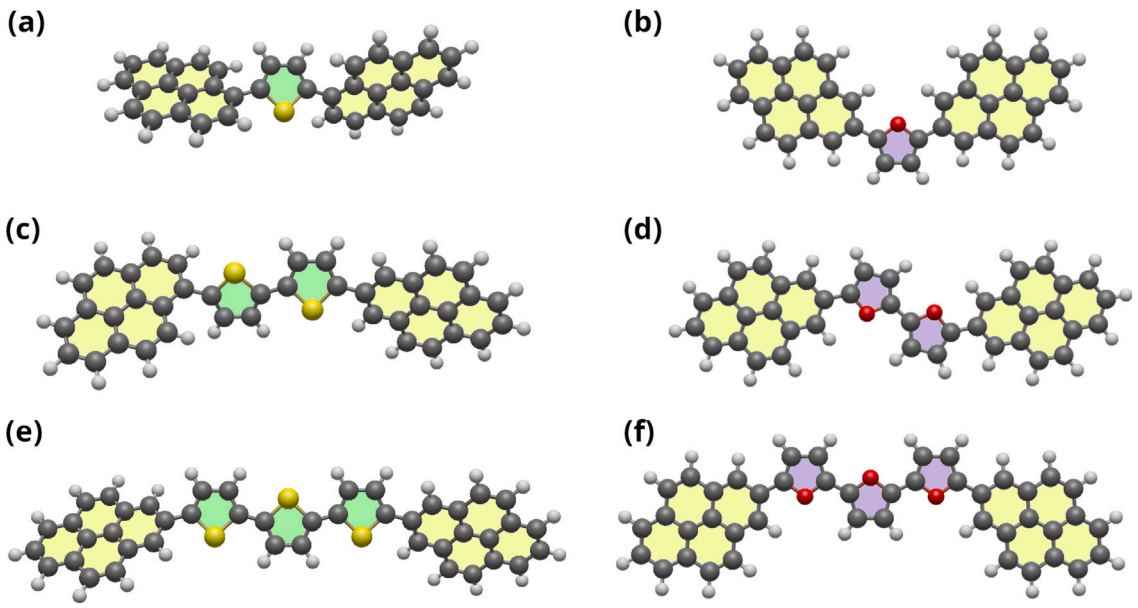


**Fig. 1.** Optimized geometries (a) BPY1T (b) BPY1F (c) BPY2T (d) BPY2F (e) BPY3T and (f) BPY3F.

**Table 1**
Molecular properties of the pyrene end-capped systems.

| System | Bond length (Å) | Bond angle (°) | MPP (Å) | SDP (Å) |
|---|---|---|---|---|
| BPY1T | 1.473 | 146.51 | 1.1516 | 3.6829 |
| BPY1F | 1.456 | 173.06 | 0.0021 | 0.0084 |
| BPY2T | 1.466 | 157.50 | 0.7594 | 3.0989 |
| BPY2F | 1.455 | 169.08 | 0.0009 | 0.0043 |
| BPY3T | 1.466 | 159.78 | 1.0086 | 3.1441 |
| BPY3F | 1.455 | 163.47 | 0.0001 | 0.0006 |

the substitution of furan, the molecules tend to be more planar than their thiophene counterparts. The corresponding bond lengths, bond angles and dihedral angles are given in Supplementary Information File (Table. S1–S6). The key bond lengths and bond angles between the pyrene and thiophene/furan core is given in Table 1. For BPY1T(F) and BPY3T(F) systems the center oxygen or sulfur atom is taken as the middle reference point. Whereas in the case of BPY2T(F) systems, a dummy atom is inserted between the two thiophene/furan rings and the angles were measured. It can be seen that by substituting furan in pyrene could results a bond length around ~1.45 Å, independent of number of furan rings in the system. In the case of thiophene, a slight reduction from 1.473 to 1.466 Å has been observed for BPY1T and BPY2T, respectively. Interestingly, additional thiophene rings does not alter the bond length between sulfur/oxygen and near by carbon atoms in the individual moieties on either side. This can be seen as the electronegativity decreases, the molecule tends to be more planar and it could lead to a minor disorientation in the case of furan systems [34].

As planarity can directly impact the mobility and ambipolarity of the OLETs, we have used an recently developed molecular planarity parameter (MPP) and span of deviation from plane (SDP) for the in-depth analysis of variation in molecular planarity with respect to the furan substitution. Details of the method can be found elsewhere [35]. In short, all the atoms in the molecule are fitted to a fitting plane by means of least squares method. Once the fitting plane is established, MPP can be obtained as the root mean square deviation of the atoms from the fitting plane. Similarly, SDP can be obtained as the difference between most positive and negative distances of an atom from the fitting plane. The difference between these parameters is that the MPP is a measure of overall deviation in atoms to the fitting plane, whereas, SDP is a deviation of the molecular span to the fitting plane. In general smaller MPP and SDP indicates more planarity in the system. The implementation in `Multiwfn` program offers the possibility to create a color map based on the deviation of atoms with respect to the fitting plane. The obtained values are given in Table 1 and the colored maps are given in the Supplementary Information File (Fig. S1). In the case of BPYT systems, BPY2T is more planar than that of the other two. Whereas for BPYF systems the molecular planarity gradually increases with increase in the number of furan rings. Further, lower SDP values in furan systems indicate a minimal twist in the system upon the substitution of rings. A similar fact is not true in the case of BPY3T. Chemically, furan derivatives are more planar than thiophene derivatives due to the higher electronegativity of oxygen than sulfur. So, lone pair electrons in the oxygen atom exerts a strong attraction to ring electrons than the sulfur, leading to strong resonance effect and more stable planar structure [36].

### 3.2. Electronic properties

The calculated frontier molecular orbitals are given in Fig. 2. It can be seen that for all the systems the electron cloud is delocalized uniformly over the entire molecule. Previously, Kazuaki Oniwa et al. have reported the theoretical HOMO (–5.54, –5.31 and –5.17), LUMO (–1.99, –2.21 and –2.36) and energy gap (3.55, 3.10 and 2.81) values for the BPY1T, BPY2T and BPY3T respectively [22]. The present values are in agreement with their report and slight variation in the values could be attributed to the choice of basis sets. The energy gap values are decreasing with the introduction of thiophene or furan ring and furan systems show slightly lower energy gap values than their thiophene counterparts. Even though there is a trend of increasing band gap values with respect to MPP and SDP, the variation is majorly due to the furan substitution. Further, the trend of increasing LUMO and decreasing HOMO with the addition of more thiophene/furan rings is an expected behavior in the case of conjugated systems due to their weak bonding and anti-bonding on the inter ring.

### 3.3. Charge injection analysis

From the frontier molecular orbital analysis, it can be seen that the HOMO and LUMO levels are in alignment with the work functions of Au and Ca, two widely used metals for the fabrication of contacts in organic semiconductor devices. This ensures the better charge injection at the source and drain levels of a practical device. But more accurate

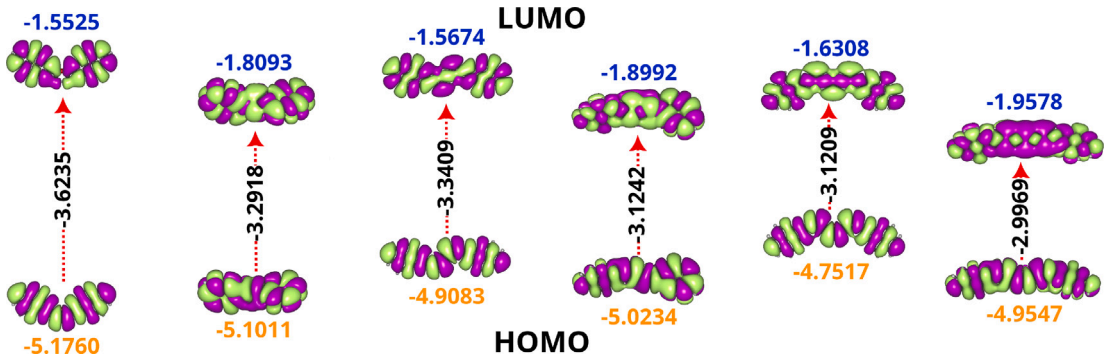


**Fig. 2.** Frontier molecular orbitals of (a) BPY1T (b) BPY1F (c) BPY2T (d) BPY2F (e) BPY3T and (f) BPY3F.

**Table 2**
Charge transport properties of pyrene end-capped systems (in eV).

| System | IP | EA | $\lambda^+$ | $\lambda^-$ | $J_e^+$ | $J_e^-$ | $\mu^+$ | $\mu^-$ |
|---|---|---|---|---|---|---|---|---|
| BPY1T | 6.027 | 0.944 | 0.345 | 0.261 | 0.010 | 0.013 | 0.002 | 0.218 |
| BPY1F | 6.229 | 0.563 | 0.109 | 0.204 | 0.007 | 0.004 | 0.120 | 0.014 |
| BPY2T | 5.929 | 1.053 | 0.326 | 0.267 | 0.010 | 0.012 | 0.087 | 0.044 |
| BPY2F | 5.916 | 0.656 | 0.087 | 0.226 | 0.008 | 0.003 | 0.092 | 0.029 |
| BPY3T | 5.834 | 1.167 | 0.340 | 0.277 | 0.012 | 0.010 | 0.035 | 0.121 |
| BPY3F | 5.712 | 0.765 | 0.141 | 0.228 | 0.008 | 0.005 | 0.090 | 0.399 |

analysis on charge injection efficiency can be done using adiabatic ionization potential (IP) and electron affinity (EA) values. Usually these IP and EA values can be related directly to the HOMO and LUMO values of the system. But, due to the exchange correlation potentials used in DFT analysis, ratio between HOMO and LUMO does not consistent with the ratio between IP and EA values [37]. On the other hand, it has been observed that the DFT values of IP and EA values are in good agreement with the experimental values. These values can be calculated using the relations,

$$IP = E_{cation} - E_{neutral} \quad (7)$$

$$EA = E_{neutral} - E_{anion} \quad (8)$$

where $E_{neutral}$, $E_{cation}$ and $E_{anion}$ are the molecular energies of neutral, cationic and anionic forms. The calculated values are given in Table 2. Usually an IP value less than 5.0 eV is considered as suitable for employing widely used Au as the electrode. Addition of more rings as well as the substitution of furan (excluding the BPY1F case) we have witnessed the decrement in IP values. This indicates the better suitability of the materials for hole injection. On the other hand, lower EA values indicates the challenge in electron injection and this could be the reason for the absence of electron transport in experimentally reported BPYT systems. Further reduction in EA values, with the introduction of furan is a concern to realize the electron transport in these systems. In real-world devices, metal contacts are often deposited on top (or bottom) of the organic semiconductor to inject and extract the charges. For efficient charge injection (or extraction), the work function of the metal should exactly match the HOMO (or LUMO) of the semiconductor. Practically, such exact matching is not always possible, and the energy difference between the work function and HOMO (or LUMO) is termed as charge injection barrier. Lower the injection barrier better would be the charge injection. In the present work, the charge injection barrier for the molecular systems with some widely used metal contacts is given in Table 3. It can be seen that the electron injection barrier for both BPYT and BPYF systems is much higher than the hole injection barrier. Due to the limited choice of materials as metal contacts, contact engineering approaches are often considered to address this issue [38].

**Table 3**
Charge injection barrier of the pyrene end-caped systems against different metals in eV.

| System | Al | | Ca | | Au | | Ag | |
|---|---|---|---|---|---|---|---|---|
| | Electron | Hole | Electron | Hole | Electron | Hole | Electron | Hole |
| BPY1FT | 2.5275 | 1.096 | 1.3475 | 2.276 | 3.5475 | 0.0760 | 3.1775 | 0.446 |
| BPY1T | 2.2707 | 1.0211 | 1.0907 | 2.2011 | 3.2907 | 0.0011 | 2.9207 | 0.371 |
| BPY2FT | 2.5126 | 0.8283 | 1.3326 | 2.0083 | 3.5326 | –0.1917 | 3.1626 | 0.178 |
| BPY2T | 2.1808 | 0.9434 | 1.0008 | 2.1234 | 3.2008 | –0.0766 | 2.8308 | 0.293 |
| BPY3FT | 2.4492 | 0.6717 | 1.2692 | 1.8517 | 3.4692 | –0.3483 | 3.0992 | 0.021 |
| BPY3T | 2.1222 | 0.8747 | 0.9422 | 2.0547 | 3.1422 | –0.1453 | 2.7722 | 0.224 |

### 3.4. Charge transfer properties

The reorganization energy ($\lambda$) and the charge transfer integral ($J_e$) are calculated using Eqs. (2) and (5) and the obtained values are given in Table 2. For higher hopping rate or charge transport, a higher transfer integral value along with lower reorganization energy is required. It can be seen that with the substitution of furan moieties the hole reorganization energies are approximately reduced by half and the $\lambda^-$ values are also significantly lesser than that of the thiophene systems.

In the present case, charge transfer integral between the dimer was estimated using the HOMO, HOMO-1 and LUMO, LUMO+1 levels, corresponding to hole and electron transfer integrals. Since these $J_e$ values indicates the coupling strength of the charge interactions, it has the major contribution to the charge transfer rates in the system. Higher $J_e$ values yields higher coupling strength and which in turn increase the charge transfer mobility. The calculated values are given in Table 2. It can be seen that with the increase in number of thiophene/furan rings, the hole transfer integral has been gradually increasing. Whereas in the case of electron transfer integrals, it is gradually decreasing with the increase in number of rings. Both reorganization energy and charge transfer integral values are used for the calculation of drift mobility. It is evident from the Table 2 that all the three thiophene system possess higher electron mobility than the hole mobility, indicating the systems are predominantly n-type materials. However, previous experimental studies reported only hole mobilities for these systems. This could be due to the choice of metal contacts utilized for the transistor fabrication. Though furan derivatives show higher hole mobilities, their electron mobilities are comparatively lower in the case of BPY1F and BPY2F systems. There were many theoretical and experimental studies where thiophene was substituted by furan shows increased hole mobility with decrease or complete loss of electron mobilities [25,26]. Though some reports claim the role of LUMO degeneracy upon furan substitution, this part has to be studied further for proper explanation [39].

### 3.5. Excited state analysis

The absorption spectra of the pyrene end-capped thiophene and furan systems are given in Fig. 3. Thiophene systems show a strong

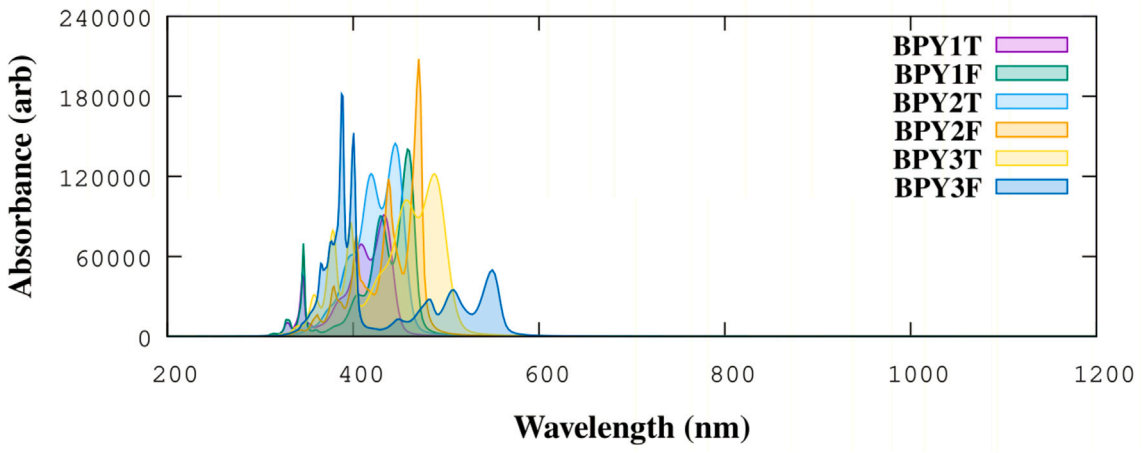


**Fig. 3.** Absorption spectrum of pyrene end-capped thiophene and furan systems.

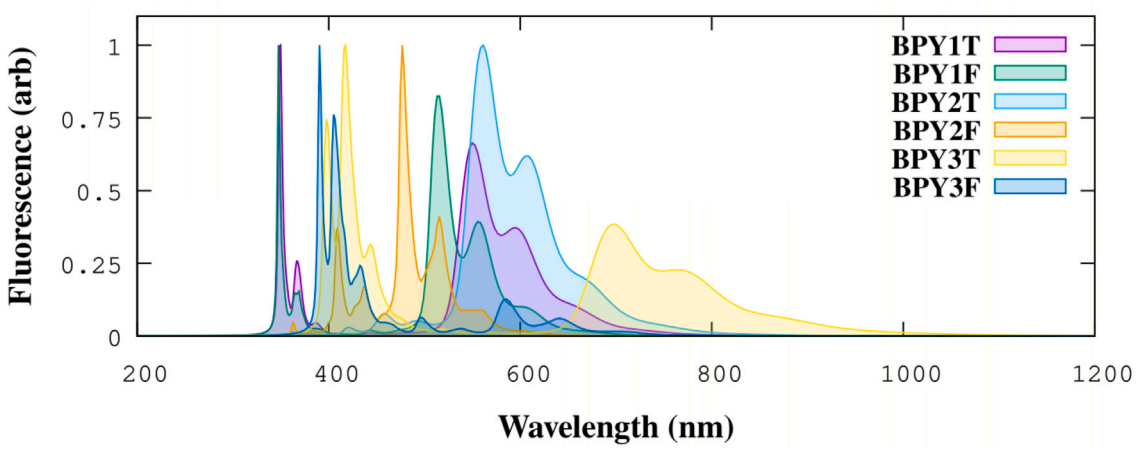


**Fig. 4.** Emission spectrum of pyrene end-capped thiophene and furan systems.

absorption band between 300 and 500 nm region, whereas furan substituted systems showing an shoulder peak in 500 nm region. Corresponding emission spectrum is given in Fig. 4. The shoulder peak in this case is broadly resolved and a dominant emission is observed in the infrared region. The emission peaks are assigned to $\pi \rightarrow \pi^*$ transition and most of their contribution arising due to LUMO → HOMO transfer. The radiation lifetime is an important parameter to be considered for the analysis of OLET systems and it can be given as

$$\tau = \frac{1.499}{f_{osc}E^2} \tag{9}$$

here E is the excitation energy, $f_{osc}$ is the oscillator strength and $\tau$ is the radiation life time. The simulated parameters and the calculated $\tau$ values are given in Table 4. It can be seen from Fig. 3 as well as from the calculated data, the electronic transition peaks are gradually red shifted owing to addition of rings in the system. Along with the radiation lifetime, the transition dipole moments (TDM) can also be used to estimate the emission efficiency. TDM measures charge displacement from the ground state to the excited state. In the case of emissive systems, higher radiative efficiencies can be obtained for the systems with larger TDM values [40]. In the present case, TDM values are slightly improving for the thiophene systems and are slightly decreasing for the furan systems, respectively. Whereas, the $\tau$ values are slightly decreasing and then increasing for thiophenes and a prompt increment is observed for furans. These variations, in the case of thiophenes can be attributed to their molecular planarity and the trend is in accordance with their corresponding MPP and SDP values. However, for furans, their larger delocalization of the excited state electron cloud along with the molecular planarity yields efficient overlap between the excited state wavefunctions, leads to better optical properties [41,42].

**Table 4**
Excited state properties of pyrene end-capped systems (in eV).

| System | E ($cm^{-1}$) | $f_{osc}$ | TDM ($au^2$) | $\tau$ (ns) |
|---|---|---|---|---|
| BPY1T | 24 200 | 1.086 | 14.776 | 2.356 |
| BPY1F | 22 685 | 1.246 | 18.090 | 2.336 |
| BPY2T | 23 638 | 1.864 | 25.963 | 1.439 |
| BPY2F | 22 406 | 1.292 | 18.985 | 2.310 |
| BPY3T | 21 646 | 1.621 | 24.658 | 1.973 |
| BPY3F | 19 381 | 0.427 | 7.261 | 9.336 |

### 3.6. Photovoltaic properties

Due to their p-type characteristics, pyrene end-capped thiophene and furan derivatives can be considered as electron donors in bulk heterojunction solar cells. In the present case, we are considering well-studied fullerene derivative ($PC_{61}BM$) as the electron acceptor [26]. Theoretically, the power conversion efficiency of an OPV can be evaluated using the parameters such as open circuit voltage ($V_{oc}$), the short circuit current density ($J_{sc}$), and the fill factor (FF). Higher these values higher would be efficiency of an OPV. The open circuit voltage can be estimated using the relation [43],

$$V_{oc} = \frac{1}{e}\left(|E_{HOMO}^{Donor}| - |E_{LUMO}^{Acceptor}|\right) - 0.3\ V \tag{10}$$

**Table 5**
Photovoltaic properties of pyrene end-capped systems.

| System | $V_{oc}$ (V) | $\eta$ (arb) | FF (%) | $E_b$ (eV) | $L_D - L_A$ (eV) |
|---|---|---|---|---|---|
| BPY1T | 1.031 | 0.943 | 88.549 | 0.569 | 1.960 |
| BPY1F | 1.106 | 0.917 | 89.150 | 0.719 | 2.217 |
| BPY2T | 0.953 | 0.948 | 87.842 | 0.435 | 1.870 |
| BPY2F | 0.838 | 0.986 | 86.597 | 0.504 | 2.202 |
| BPY3T | 0.884 | 0.626 | 87.132 | 0.671 | 1.812 |
| BPY3F | 0.681 | 0.976 | 84.364 | 0.523 | 2.139 |

Here e is the elementary charge, $|E_{HOMO}^{Donor}|$ and $|E_{LUMO}^{Acceptor}|$ are absolute value of HOMO of the donor and LUMO of the acceptor systems. For $PC_{61}BM$ the LUMO value is about –3.77 eV. The obtained values are given in Table 5. It can be seen that the $V_{oc}$ values decreases with increase in number of oligomeric rings. Further, the furan substitution has a positive impact only in the case of BPY1F, whereas for the other systems $V_{oc}$ values has been substantially decreased.

The light harvesting efficiency of the system can be related to the short circuit current density $J_{sc}$ using the relation,

$$J_{sc} = q \int_0^{\infty} Sun(\lambda)\ \eta(\lambda)\ IQE(\lambda)\ d(\lambda) \tag{11}$$

where, $Sun(\lambda)$ is the spectral irradiance of the incident light, $\eta(\lambda)$ is the light absorbing efficiency of the system, and $IQE(\lambda)$ is the internal quantum efficiency. In an ideal situation, the $\eta(\lambda)$ values are directly proportional to $J_{sc}$. So, the $\eta(\lambda)$ values are calculated from the simulated absorption spectrum for the major peaks using,

$$\eta_{\lambda} = 1 - 10^{-f_{osc}} \tag{12}$$

The calculated values are given in Table 5. With increase in number of oligomeric rings the harvesting efficiency of the thiophene derivatives gradually decreases whereas in the case of furan systems, an improvement has been observed.

Finally, the fill factor can be calculated by

$$FF = \frac{\upsilon_{oc} - \ln(\upsilon_{oc} + 0.72)}{\upsilon_{oc} + 1} \tag{13}$$

where $\upsilon_{oc}$ can be given as,

$$\upsilon_{oc} = \frac{eV_{oc}}{k_B T} \tag{14}$$

The accuracy of Eq. (13) is said to have valid, if the values are greater than 10%. In the present case we have obtained values around 85% and are given in Table 5. The FF values are gradually decreasing with the increment in number of rings in both thiophene and furan systems. Further, the charge transfer behavior of specific OPVs can be estimated using exciton binding energy and the energetic driving force. The exciton binding energy is the energy required to dissociate an exciton into electron and hole. Lower these values, easier it would be to obtain the free charges. It can be calculated as the difference between frontier orbital gap ($E_g$) and the exciton energy of the first singlet ($E_{opt}$) as,

$$E_b = E_g - E_{opt} \tag{15}$$

The calculated values are given in Table 5. The values are gradually decreasing with increase up to two rings. Further $E_b$ values are higher for furan substituted systems than their thiophene counterparts. For both BPY3T and BPY3F the values are slightly increasing owing to their orbital degeneracy due to the additional ring. The energetic driving force ($L_D - L_A$) is the energy difference between LUMO of donor and acceptor and are given in Table 5. The values indicate that there is enough driving force for efficient charge separation at donor level. Further, lower $E_b$ values than the $L_D - L_A$ suggests the higher possibility of exciton dissociation in the system.

In the case of $V_{oc}$ and FF, the values are decreasing with respect to the increase in number of rings. This is due to the more charge delocalization with the addition of rings in both the systems, such delocalization advantageous in the sense of OLETs. However, in the case of thiophene systems, the molecular planarity plays a crucial role as its MPP and SDP increases, especially for BPY3T system. Furan seems to have an positive impact in the sense of light absorption as it has lower torsional angle bending leading to more rigidity.

A note of caution is, in the present case, all the calculations are carried out for the gas phase molecular systems. Though the frontier molecular orbitals and the spectral properties can be directly inferred with the real chemical systems, the choice of the functional and the basis sets would impact their accuracy. As discussed in the Electronic Properties, a slight variation in the values of frontier molecular orbitals with respect to the choice of basis set between the present work and Kazuaki Oniwa et al. report is worth mentioning here [22]. Additionally, the calculated drift mobilities are for the dimers and are entirely different from the solid-state field effect mobilities calculated using OFETs and OLETs. So, it is wise to avoid directly comparing the experimental mobility values with the simulated values. Nevertheless, the observed drift mobility trend for different oligomeric lengths and substitutions should result in similar physical phenomena. So, a similar improvement or decrement can be expected in the experimental data.

## 4. Conclusions

Pyrene end-capped thiophene and furan derivatives are studied using density functional theory at the level of B3LYP and 6-311G(d,p) basis set. From the geometrical parameters and the molecular planarity analysis it is evident that upon furan substitution the molecule tends to be more planar. This has an impact on the electronic and optical properties of the furan substituted systems. Considering the charge injection barrier, furan substituted systems shows shorter band gaps and higher hole mobility than their thiophene counterparts. On the other hand, furan substitution substantially affect the electron mobility, which seems to be an universal behavior in these systems. All the systems show both electron and hole transfer characteristics but much experimental work is required in terms of contact engineering to realize ambipolar mobility. In the case of photovoltaic analysis, the furan substitution greatly improves the light harvesting efficiency. On the other hand, short circuit voltage and fill factors are slightly affected upon increasing the number of rings in both systems.

## CRediT authorship contribution statement

**Arka Bhattacharya:** Methodology, Software, Validation, Formal analysis, Writing – review & editing. **Periyasamy Angamuthu Praveen:** Conceptualization, Methodology, Software, Validation, Investigation, Writing – original draft, Writing – review & editing, Visualization, Project administration. **Sreegowri V. Bhat:** Formal analysis, Data curation, Writing – review & editing. **Saravanapriya Dhanapal:** Formal analysis, Data curation, Writing – review & editing. **Arulkannan Kandhasamy:** Formal analysis, Data curation, Writing – review & editing. **Thangavel Kanagasekaran:** Conceptualization, Methodology, Validation, Resources, Writing – original draft, Writing – review & editing, Supervision, Funding acquisition.

## Declaration of competing interest

The authors declare that they have no known competing financial interests or personal relationships that could have appeared to influence the work reported in this paper.

## Data availability

Given as the supplementary information file

## Acknowledgments

This work was supported by SERB CRG grant by Govt. of India (CRG/2022/006100). Further, AB acknowledges the financial support from Department of Science and Technology, India, in the form of DST INSPIRE fellowship (IF170616). PP thank the Indian Institute of Science Education and Research - Tirupati for the financial support. The authors acknowledge the support and help from the IT department, IISER-Tirupati for computational facilities.

## Appendix A. Supplementary data

Supplementary material related to this article can be found online at https://doi.org/10.1016/j.comptc.2023.114135.

## References

[1] X. Xu, Y. Zhao, Y. Liu, Wearable electronics based on stretchable organic semiconductors, Small (2023) 2206309.
[2] H. Ren, J.-D. Chen, Y.-Q. Li, J.-X. Tang, Recent progress in organic photodetectors and their applications, Adv. Sci. 8 (1) (2021) 2002418.
[3] S. Yu, C.J. Kousseff, C.B. Nielsen, n-Type semiconductors for organic electrochemical transistor applications, Synth. Met. 293 (2023) 117295.
[4] Q. Liu, S.E. Bottle, P. Sonar, Developments of diketopyrrolopyrrole-dye-based organic semiconductors for a wide range of applications in electronics, Adv. Mater. 32 (4) (2020) 1903882.
[5] D. Patra, S. Park, Solution processable benzotrithiophene (BTT)-based organic semiconductors: Recent advances and review, Macromol. Rapid Commun. 43 (21) (2022) 2200473.
[6] H. Gao, J. Liu, Z. Qin, T. Wang, C. Gao, H. Dong, W. Hu, High-performance amorphous organic semiconductor-based vertical field-effect transistors and light-emitting transistors, Nanoscale 12 (35) (2020) 18371–18378.
[7] Z. Qin, H. Gao, H. Dong, W. Hu, Organic light-emitting transistors entering a new development stage, Adv. Mater. 33 (31) (2021) 2007149.
[8] K. Wang, Y.S. Zhao, Pursuing electrically pumped lasing with organic semiconductors, Chem 7 (12) (2021) 3221–3231.
[9] J. Lee, S.A. Park, S.U. Ryu, D. Chung, T. Park, S.Y. Son, Green-solvent-processable organic semiconductors and future directions for advanced organic electronics, J. Mater. Chem. A 8 (41) (2020) 21455–21473.
[10] M. Liu, P. Fan, Q. Hu, T.P. Russell, Y. Liu, Naphthalene-diimide-based ionenes as universal interlayers for efficient organic solar cells, Angew. Chem. 132 (41) (2020) 18288–18292.
[11] Y. Liu, P. Cheng, T. Li, R. Wang, Y. Li, S.-Y. Chang, Y. Zhu, H.-W. Cheng, K.-H. Wei, X. Zhan, et al., Unraveling sunlight by transparent organic semiconductors toward photovoltaic and photosynthesis, ACS Nano 13 (2) (2019) 1071–1077.
[12] H. Shang, H. Shimotani, T. Kanagasekaran, K. Tanigaki, Separation in the roles of carrier transport and light emission in light-emitting organic transistors with a bilayer configuration, ACS Appl. Mater. Interfaces 11 (22) (2019) 20200–20204.
[13] X. Shen, Y. Wang, J. Li, Y. Chen, Z. Wang, W. Wang, L. Huang, L. Chi, Performances of pentacene OFETs deposited by arbitrary mounting angle vacuum evaporator, Front. Mater. 7 (2020) 245.
[14] B. Amna, R. Isci, H.M. Siddiqi, L.A. Majewski, S. Faraji, T. Ozturk, High-performance, low-voltage organic field-effect transistors using thieno [3, 2-b] thiophene and benzothiadiazole co-polymers, J. Mater. Chem. C 10 (21) (2022) 8254–8265.
[15] S.N. Afraj, G.-Y. He, C.-Y. Lin, A. Velusamy, C.-Y. Huang, P.-S. Lin, S. Vegiraju, P.-Y. Huang, J.-S. Ni, S.-L. Yau, et al., Solution-processable multifused thiophene small molecules and conjugated polymer semiconducting blend for organic field effect transistor application, Adv. Mater. Technol. 6 (3) (2021) 2001028.
[16] F. Sasaki, S. Dokiya, H. Yanagi, Optically pumped lasing of cyano-substituted thiophene/phenylene co-oligomer microcrystals fabricated by the slide boat method, Japan. J. Appl. Phys. 58 (SB) (2019) SBBG05.
[17] W. Waliszewski, Z.S. Parr, A. Michalska, R. Halaksa, H. Zajaczkowska, P. Sleczkowski, M. Neophytou, B. Luszczynska, P.W. Blom, C.B. Nielsen, et al., Role of oxygen within end group substituents on film morphology and charge carrier transport in thiophene/phenylene small-molecule semiconductors, Org. Electron. 109 (2022) 106608.
[18] P.A. Praveen, A. Bhattacharya, T. Kanagasekaran, A DFT study on the electronic and photophysical properties of biphenylyl/thiophene derivatives for organic light emitting transistors, Mater. Today Commun. 25 (2020) 101509.
[19] P.A. Praveen, P. Muthuraja, P. Gopinath, T. Kanagasekaran, Impact of furan substitution on the optoelectronic properties of biphenylyl/thiophene derivatives for light-emitting transistors, J. Phys. Chem. A 126 (4) (2022) 600–607.
[20] M.I. Nan, E. Lakatos, G.-I. Giurgi, L. Szolga, R. Po, A. Terec, S. Jungsuttiwong, I. Grosu, J. Roncali, Mono-and di-substituted pyrene-based donor-$\pi$-acceptor systems with phenyl and thienyl $\pi$-conjugating bridges, Dye. Pigment. 181 (2020) 108527.
[21] T.M. Pathiranage, Z. Ma, C.M. Udamulle Gedara, X. Pan, Y. Lee, E.D. Gomez, M.C. Biewer, K. Matyjaszewski, M.C. Stefan, Improved self-assembly of P3HT with pyrene-functionalized methacrylates, ACS Omega 6 (41) (2021) 27325–27334.
[22] K. Oniwa, H. Kikuchi, H. Shimotani, S. Ikeda, N. Asao, Y. Yamamoto, K. Tanigaki, T. Jin, 2-Positional pyrene end-capped oligothiophenes for high performance organic field effect transistors, Chem. Commun. 52 (26) (2016) 4800–4803.
[23] J. Kwon, J.-P. Hong, S. Noh, T.-M. Kim, J.-J. Kim, C. Lee, S. Lee, J.-I. Hong, Pyrene end-capped oligothiophene derivatives for organic thin-film transistors and organic solar cells, New J. Chem. 36 (9) (2012) 1813–1818.
[24] X. Jin, L. Sun, D. Li, C.-L. Wang, F.-Q. Bai, Efficiency difference between furan- and thiophene-based D–$\pi$–A dyes in DSSCs explained by theoretical calculations, RSC Adv. 8 (52) (2018) 29917–29923.
[25] H. Cao, P.A. Rupar, Recent advances in conjugated furans, Chem. Eur. J. 23 (59) (2017) 14670–14675.
[26] B. Zheng, L. Huo, Recent advances of furan and its derivatives based semiconductor materials for organic photovoltaics, Small Methods 5 (9) (2021) 2100493.
[27] S.A. Siddiqui, In silico investigation of the coumarin-based organic semiconductors for the possible use in organic electronic devices, J. Phys. Org. Chem. 32 (3) (2019) e3905.
[28] J. Bertrandie, J. Han, C.S. De Castro, E. Yengel, J. Gorenflot, T. Anthopoulos, F. Laquai, A. Sharma, D. Baran, The energy level conundrum of organic semiconductors in solar cells, Adv. Mater. 34 (35) (2022) 2202575.
[29] D.M. Mamand, H.M. Qadr, Comprehensive spectroscopic and optoelectronic properties of bbl organic semiconductor, Prot. Met. Phys. Chem. Surf. 57 (2021) 943–953.
[30] Y.-C. Chang, M.-Y. Kuo, C.-P. Chen, H.-F. Lu, I. Chao, On the air stability of n-channel organic field-effect transistors: a theoretical study of adiabatic electron affinities of organic semiconductors, J. Phys. Chem. C 114 (26) (2010) 11595–11601.
[31] T.P. Nguyen, J.H. Shim, J.Y. Lee, Density functional theory studies of hole mobility in picene and pentacene crystals, J. Phys. Chem. C 119 (21) (2015) 11301–11310.
[32] X. Wang, K.-C. Lau, Theoretical investigations on charge-transfer properties of novel high mobility n-channel organic semiconductors–diazapentacene derivatives, J. Phys. Chem. C 116 (43) (2012) 22749–22758.
[33] T. Petrenko, F. Neese, Analysis and prediction of absorption band shapes, fluorescence band shapes, resonance Raman intensities, and excitation profiles using the time-dependent theory of electronic spectroscopy, J. Chem. Phys. 127 (16) (2007) 164319.
[34] J.E. Huheey, Bent's rule: energetics, electronegativity, and the structures of nonmetal fluorides, Inorg. Chem. 20 (11) (1981) 4033–4035.
[35] T. Lu, Simple, reliable, and universal metrics of molecular planarity, J. Mol. Model. 27 (9) (2021) 263.
[36] Z. Zhao, H. Nie, C. Ge, Y. Cai, Y. Xiong, J. Qi, W. Wu, R.T. Kwok, X. Gao, A. Qin, et al., Furan is superior to thiophene: a furan-cored AIEgen with remarkable chromism and OLED performance, Adv. Sci. 4 (8) (2017) 1700005.
[37] G. Gogoi, L. Bhattacharya, S. Rahman, N.S. Sarma, S. Sahu, B.K. Rajbongshi, S. Sharma, New donor-acceptor-donor type of organic semiconductors based on the regioisomers of diketopyrrolopyrroles: A DFT study, Mater. Today Commun. 25 (2020) 101364.
[38] T. Kanagasekaran, H. Shimotani, R. Shimizu, T. Hitosugi, K. Tanigaki, A new electrode design for ambipolar injection in organic semiconductors, Nature Commun. 8 (1) (2017) 999.
[39] A.D. Hendsbee, J.-P. Sun, T.M. McCormick, I.G. Hill, G.C. Welch, Unusual loss of electron mobility upon furan for thiophene substitution in a molecular semiconductor, Org. Electron. 18 (2015) 118–125.
[40] Z. Wei, S. Jiang, F. Qi, X. Lv, J. Song, J. Gu, L. Meng, C.-Z. Lu, Predicting and designing thermally activated delayed fluorescence molecules with balanced $\Delta$EST and transition dipole moment, Adv. Theory Simul. 5 (11) (2022) 2200494.
[41] I.P. Koskin, E.A. Mostovich, E. Benassi, M.S. Kazantsev, Way to highly emissive materials: Increase of rigidity by introduction of a furan moiety in co-oligomers, J. Phys. Chem. C 121 (42) (2017) 23359–23369.
[42] H. Karabıyık, G.Ö. Ürüt, R. Sevinçek, Excited state aromatization assisted push-pull abilities of two unsaturated oxazolone derivatives, J. Saudi Chem. Soc. 22 (5) (2018) 519–526.
[43] Z. Fu, W. Shen, R. He, X. Liu, H. Sun, W. Yin, M. Li, Theoretical studies on the effect of a bithiophene bridge with different substituent groups (R=H, CH 3, OCH 3 and CN) in donor–$\pi$–acceptor copolymers for organic solar cell applications, Phys. Chem. Chem. Phys. 17 (3) (2015) 2043–2053.